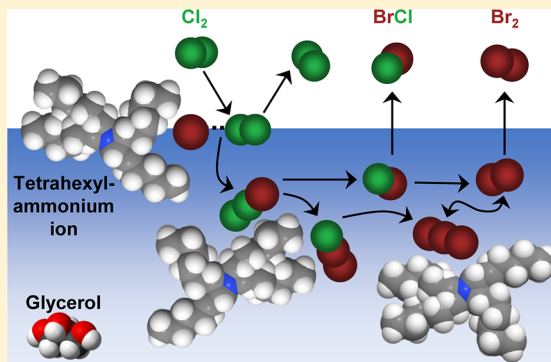


# Surfactant-Promoted Reactions of $\text{Cl}_2$ and $\text{Br}_2$ with $\text{Br}^-$ in Glycerol

Jennifer A. Faust, Logan P. Dempsey, and Gilbert M. Nathanson\*

Department of Chemistry, University of Wisconsin—Madison, 1101 University Avenue, Madison, Wisconsin 53706-1322, United States

**ABSTRACT:** Gas–liquid scattering experiments are used to explore reactions of gaseous  $\text{Cl}_2$  and  $\text{Br}_2$  with a 0.03 M solution of the surfactant tetrahexylammonium bromide (THABr) dissolved in glycerol. At thermal collision energies,  $79 \pm 2\%$  of incident  $\text{Cl}_2$  molecules react with  $\text{Br}^-$  to form  $\text{Cl}_2\text{Br}^-$  in the interfacial region. This reaction probability is three times greater than the reactivity of  $\text{Cl}_2$  with 3 M NaBr–glycerol, even though the interfacial  $\text{Br}^-$  concentrations are similar in each solution. We attribute the high 79% uptake to the presence of surface  $\text{THA}^+$  ions that stabilize the  $\text{Cl}_2\text{Br}^-$  intermediate as it is formed in the charged, hydrophobic pocket created by the hexyl chains.  $\text{Cl}_2\text{Br}^-$  generates the single exchange product  $\text{BrCl}$  in a 1% yield close to the surface, while the remaining 99% desorbs as the double exchange product  $\text{Br}_2$  over  $>0.1$  s after diffusing deeply into the bulk. When NaCl is added to the surfactant solution in a 20:1  $\text{Cl}^-/\text{Br}^-$  ratio, the  $\text{Cl}_2$  reaction probability drops from 79% to  $46 \pm 1\%$ , indicating that  $\text{Cl}^-$  in the interfacial region only partially blocks reaction with  $\text{Br}^-$ . In parallel, we observe that gaseous  $\text{Br}_2$  molecules dissolve in 0.03 M THABr for  $10^4$  times longer than in 3 M NaBr. We attribute this change to formation of stabilizing interfacial and bulk-phase  $\text{THA}^+\text{Br}_3^-$  ion pairs, in analogy with the capture of  $\text{Cl}_2$  and formation of  $\text{THA}^+\text{Cl}_2\text{Br}^-$  pairs. The  $\text{THA}^+$  ion appears to be a powerful interfacial catalyst for promoting reaction of  $\text{Cl}_2$  and  $\text{Br}_2$  with  $\text{Br}^-$  and for ferrying the resultant ions into solution.



## INTRODUCTION

Surface-active molecules can dramatically alter interactions between gases and liquids, in part because these “frontier” species may react first with incoming gas-phase molecules, enhance their interfacial solubility, facilitate or hinder transport, or physically block their entry into the bulk.<sup>1–9</sup> One class of soluble, cationic surfactants are the tetraalkylammonium (TAA) salts, which readily segregate to the surface of protic liquids.<sup>10–12</sup> Frequently used as phase transfer catalysts, TAA ions straddle the interface between solvents of different polarity and ferry reactant and product ions between the solvents.<sup>13,14</sup> The investigations below demonstrate that tetrahexylammonium ( $\text{THA}^+$ ) ions can also dramatically enhance gas–liquid reactions, in particular by promoting halogen atom exchange between gaseous  $\text{Cl}_2$  and interfacial  $\text{Br}^-$  ions and by extending the lifetime of the  $\text{Br}_2$  product in solution.

Experimental and theoretical studies confirm that large, polarizable anions such as  $\text{Br}^-$  are present at the gas–liquid interface,<sup>15–18</sup> especially when they are associated with surfactant counterions.<sup>10,12,19</sup> Hu et al. first implicated surface kinetics in the reaction of gaseous  $\text{Cl}_2$  and  $\text{Br}_2$  with interfacial  $\text{Br}^-$  and  $\text{I}^-$  ions in aqueous NaBr and NaI solutions.<sup>20</sup> Subsequent studies identified other interfacial reactions of halide ions, including  $\text{OH} + \text{Cl}^-$ ,<sup>21</sup>  $\text{BrCl} + \text{I}^-$ ,<sup>22</sup> and  $\text{O}_3 + \text{Br}^-$  and  $\text{I}^-$ .<sup>4,23,24</sup> We focus here on the halogen atom exchange reactions  $\text{Cl}_2 + \text{Br}^- \rightarrow \text{BrCl} + \text{Cl}^-$  and  $\text{Cl}_2 + 2\text{Br}^- \rightarrow \text{Br}_2 + 2\text{Cl}^-$ , depicted in Figure 1. These reaction pathways, proceeding through the intermediates  $\text{Cl}_2\text{Br}^-$ ,  $\text{Br}_2\text{Cl}^-$ , and

$\text{Br}_3^-$ , are based on earlier studies in salty water<sup>25,26</sup> and glycerol.<sup>27</sup> Reactions between  $\text{Cl}_2$  and  $\text{Br}^-$  have also been investigated in the gas phase<sup>28</sup> and at the surfaces of ice<sup>29</sup> and solid alkali halides.<sup>30,31</sup>

Halogen exchange reactions are of atmospheric interest because  $\text{Br}_2$  released from sea spray, snowpack, and sea ice may contribute to tropospheric ozone destruction through autocatalytic reactions known as the “bromine explosion”.<sup>32,33</sup> The reaction sequence involves  $\text{Br}_2$  photolysis, which generates Br atoms that react with  $\text{O}_3$  to form  $\text{BrO}$ . Br and  $\text{BrO}$  may then oxidize elemental Hg into  $\text{HgBr}$ ,  $\text{HgBrO}$ , and  $\text{HgO}$ , which deposit into the Arctic ecosystem.<sup>33</sup> It may even be possible that surfactant ions enhance ozone depletion and Hg deposition by drawing more  $\text{Br}^-$  ions to the surface of sea spray. In a separate context, an understanding of the interactions of  $\text{Br}_2$  with TAA salts is important in designing zinc–bromine batteries, where TAA salts are used as  $\text{Br}_2$  complexing agents to prevent the release of gaseous  $\text{Br}_2$ .<sup>34</sup>

We seek a molecular-level understanding of surfactant-enhanced reactions of  $\text{Cl}_2$  and  $\text{Br}_2$  with  $\text{Br}^-$  by using gas–liquid scattering experiments to explore reactions of these gases with a 0.03 M THABr–glycerol solution. This THABr concentration is just below the value that produces a two-phase system.<sup>11</sup> A comparison with earlier experiments using 3 M NaBr–

Received: August 7, 2013

Revised: September 16, 2013

Published: September 17, 2013

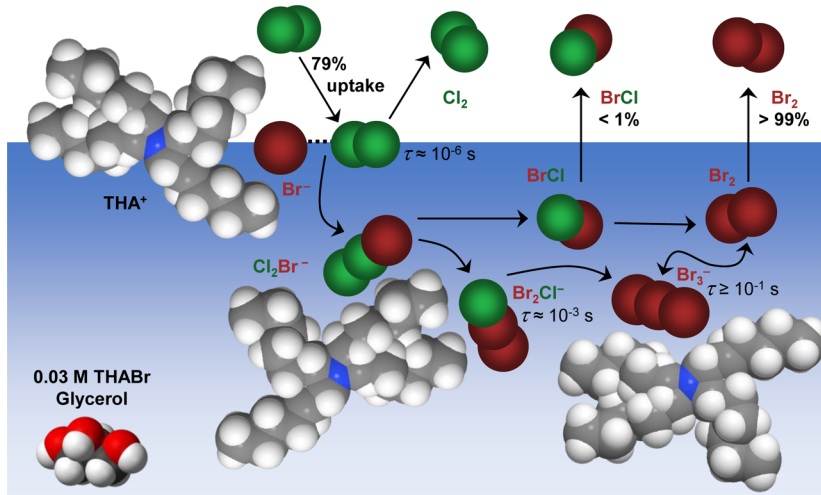


**Figure 1.** One of many possible scenarios depicting formation of  $\text{Cl}_2\text{Br}^-$  in the pocket of a surface tetrahexylammonium ( $\text{THA}^+$ ) ion. The subsequent reactions to produce  $\text{BrCl}$  and  $\text{Br}_2$  will also occur in close proximity to surface and bulk-phase  $\text{THA}^+$  ions. This complexation by  $\text{THA}^+$  increases the uptake of  $\text{Cl}_2$  by 3-fold and the characteristic lifetime ( $\tau$ ) of  $\text{Br}_3^-$  by at least  $10^4$ -fold in 0.03 M THABr–glycerol relative to 3 M NaBr–glycerol.

glycerol<sup>27</sup> provides a way to isolate the effect of the  $\text{THA}^+$  surfactant on interfacial halogen exchange. The solvent for both solutions is glycerol [ $\text{HOCH}_2\text{CH}(\text{OH})\text{CH}_2\text{OH}$ ], a protic liquid that is ideal for vacuum-based experiments because of its low vapor pressure ( $10^{-4}$  Torr). Glycerol shares many properties with water, including similar solubilities of many salts, the capacity to hydrogen bond, and a high surface tension of  $63 \text{ dyn cm}^{-1}$ .<sup>35</sup>

Previous surface tension measurements of 0.03 M THABr–glycerol,<sup>11</sup> coupled with the Gibbs equation for monolayer adsorption, reveal that the surface concentrations are  $\sim 8 \times 10^{13} \text{ cm}^{-2}$  for  $\text{THA}^+$  and  $\text{Br}^-$  and  $\sim 16 \times 10^{13} \text{ cm}^{-2}$  for glycerol.<sup>36</sup> These values correspond to about one glycerol molecule for each ion and fractional surface areas of  $\sim 8\%$   $\text{Br}^-$  ions, 55%  $\text{THA}^+$  ions, and 37% glycerol molecules. By comparison, the surface concentrations of  $\text{Na}^+$  and  $\text{Br}^-$  in 3 M NaBr–glycerol are calculated to be  $\sim 7 \times 10^{13} \text{ cm}^{-2}$ , corresponding to  $\sim 7\%$   $\text{Br}^-$ , 3%  $\text{Na}^+$ , and 90% glycerol.<sup>11</sup> Even though the two solutions have similar interfacial  $\text{Br}^-$  concentrations of  $(7\text{--}8) \times 10^{13} \text{ cm}^{-2}$ , the measurements below indicate that the uptake of  $\text{Cl}_2$  is more than three times greater into the  $\text{THA}^+$  solution than into the  $\text{Na}^+$  solution. We propose that  $\text{THA}^+$  promotes this high reactivity by creating a solvent-excluding, positively charged region at the surface, depicted in Figure 1, that traps  $\text{Cl}_2\text{Br}^-$  as it forms in the initial reaction between  $\text{Cl}_2$  and  $\text{Br}^-$ .

## EXPERIMENTAL METHODS

The surfactant and salt solutions are prepared by adding THABr (Aldrich, 99%), THACl (Aldrich, 96%), TEABr (tetraethylammonium bromide, Aldrich, 99%), NaBr (Aldrich, 99.0%), or NaCl (Aldrich, 99.0%) to glycerol (Aldrich, 99%) while degassing under low vacuum with gentle stirring and heating.<sup>27</sup> Continuously renewed liquid films are created within the reservoir shown in Figure 2 by rotating a partially submerged 5 cm diameter glass wheel through the solutions, each cooled to  $T_{\text{liq}} = 290 \text{ K}$ . The vertical films are then scraped to a uniform thickness of 0.3 mm using a Teflon bar before being exposed to vacuum through a  $12 \times 6 \text{ mm}^2$  window in the reservoir, where they are intercepted by beams of Ar,  $\text{Cl}_2$ , or  $\text{Br}_2$  at an incident angle of  $45^\circ$ . The exposure time  $t_{\text{exp}}$  of the liquid

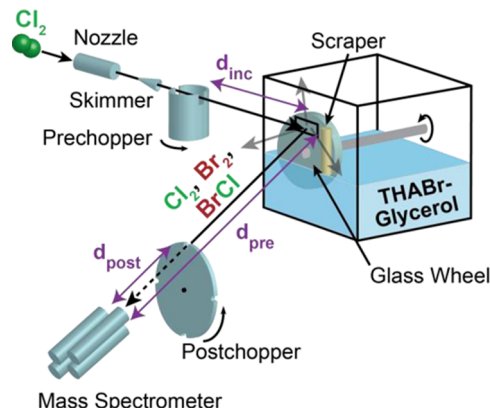


**Figure 2.** Gas–liquid scattering apparatus. The pre- and postchopper wheels are used in separate experiments to measure velocity and residence time distributions, respectively.

to the incident beams can be varied from 0.047 to 0.47 s by changing the rotation speed of the glass wheel, but it is set to 0.12 s unless noted.

The gas beams are prepared by supersonically expanding 2%  $\text{Ar}/\text{H}_2$ , 3%  $\text{Cl}_2/\text{He}$ , or 5%  $\text{Cl}_2/\text{Ar}$  through a  $100 \mu\text{m}$  diameter nozzle heated to 395 K at a backing pressure of 500 Torr. The respective beam energies are  $90 \pm 8$ ,  $58 \pm 6$ , and  $12 \pm 1 \text{ kJ mol}^{-1}$ . Cluster formation in each beam is measured to be negligible.<sup>27</sup> A higher energy  $\text{Cl}_2$  beam is prepared by passing  $\text{H}_2$  through a mixture of  $\text{KMnO}_4(s)$  and 12 M  $\text{HCl(aq)}$ , generating  $\text{Cl}_2$  molecules with a translational energy estimated to be  $\sim 100 \text{ kJ mol}^{-1}$ . A high-energy  $\text{Br}_2$  beam, estimated to be  $150 \text{ kJ mol}^{-1}$ , is prepared by passing  $\text{H}_2$  over frozen  $\text{Br}_2$  at 243 K.

As shown in Figure 2, molecules that scatter or desorb from the liquid are detected by a quadrupole mass spectrometer at a  $45^\circ$  exit angle. The gas beam is chopped into pulses by either the spinning postchopper or prechopper wheel. In the postchopper mode, reactant  $\text{Cl}_2$  molecules strike the liquid continuously. The scattered  $\text{Cl}_2$  or desorbing  $\text{BrCl}$  and  $\text{Br}_2$  products are then sliced into  $80 \mu\text{s}$  pulses. These molecules travel a distance  $d_{\text{post}} = 19.4 \text{ cm}$  to the ionizer of the mass

spectrometer, where their arrival times are recorded in a time-of-flight (TOF) spectrum. In the prechopper mode, the  $\text{Cl}_2$  beam is sliced into  $80\ \mu\text{s}$  pulses and traverses a distance  $d_{\text{inc}} = 6.8\ \text{cm}$  before striking the liquid. Desorbing and scattered molecules then travel  $d_{\text{pre}} = 25.4\ \text{cm}$  to the mass spectrometer. Their total arrival time is the sum of the flight time for the reactant to travel from the prechopper wheel to the liquid; the residence time of the reactant, intermediates, and product in solution; and the flight time for the desorbing product to reach the mass spectrometer. The prechopper technique can be used to measure residence times between  $10^{-6}$  and  $10^{-1}\ \text{s}$ .<sup>37</sup>

## RESULTS AND ANALYSIS

A search for reaction products indicates that  $\text{BrCl}$  and  $\text{Br}_2$  desorb from THABr–glycerol upon exposure to  $\text{Cl}_2$ . No  $\text{HBr}$ ,  $\text{HCl}$ ,  $\text{HOCl}$ , or  $\text{HOBr}$  were detected from the solution. The absence of these products implies that  $\text{Cl}_2$  does not react directly with  $\text{THA}^+$  ions, at least to produce volatile products,<sup>38</sup> and no products were detected from reactions of  $\text{Cl}_2$  with pure glycerol.<sup>27</sup> To investigate halogen exchange processes that produce  $\text{BrCl}$  and  $\text{Br}_2$ , we measured the uptake of  $\text{Cl}_2$  into THABr–glycerol, the branching fractions of  $\text{BrCl}$  and  $\text{Br}_2$  products, the residence times of  $\text{Cl}_2$  and  $\text{Br}_2$  incident on the solution, and the time scales for desorption of  $\text{BrCl}$  and  $\text{Br}_2$  products. Additional  $\text{Br}_2$  scattering experiments were performed to measure its lifetime in other glycerol-surfactant solutions.  $\text{Cl}_2$  scattering experiments were also performed using a mixed 0.6 M NaCl–0.03 M THABr–glycerol solution to determine the influence of interfacial  $\text{Cl}^-$  ions on  $\text{Cl}_2$  reactivity.

**Characterization of THABr–Glycerol Surface.** We use high-energy Ar scattering as a probe of the surface composition of the THABr solution. The two main pathways for interactions of inert gases such as Ar with the liquid surface are shown in Figure 3: direct inelastic scattering (IS) and trapping followed by thermal desorption (TD). Ar atoms that scatter inelastically undergo one or a few bounces along the surface but retain much of their incident energy and desorb with high velocities, arriving at the mass spectrometer at early times. Ar atoms that undergo trapping and desorption fully dissipate their incident

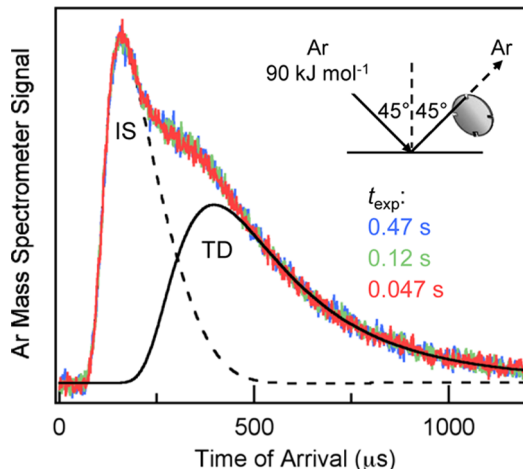


**Figure 3.** Postchopper spectra of  $90\ \text{kJ mol}^{-1}$  Ar scattering from  $0.03\ \text{M}$  THABr–glycerol at  $t_{\text{exp}} = 0.047\ \text{s}$  (red),  $0.12\ \text{s}$  (yellow), and  $0.47\ \text{s}$  (blue). Atoms that inelastically scatter (IS) from the solution arrive earlier (because of higher velocities) than those that thermally desorb (TD). The solid black line is a Maxwell–Boltzmann (MB) distribution at  $T_{\text{liq}}$  and the dashed line is a fit to the IS component.

energy into the liquid and desorb with a broad velocity distribution that is well fit by a Maxwell–Boltzmann (MB) distribution at  $T_{\text{liq}}$ . The Ar recoil energy and branching between the IS and TD pathways change with the identity of the species at the surface and therefore provide a probe of its composition. In previous experiments, we compared high-energy Ar scattering from pure glycerol and THABr–glycerol.<sup>11</sup> The TD/IS ratio was greater in the surfactant-coated solution than in pure glycerol, most likely because the hexyl chains of  $\text{THA}^+$  ions roughen the surface and promote multiple bounces of the Ar atoms. Here we investigated the time required for THABr to segregate to the surface by recording Ar TOF spectra at exposure times of  $0.047$ ,  $0.12$ , and  $0.47\ \text{s}$ , as shown in Figure 3. The three spectra are identical, confirming that THABr rises to the surface in less than  $0.047\ \text{s}$  and that the surface composition is constant up to  $0.47\ \text{s}$ .

**Cl<sub>2</sub> Uptake into 0.03 M THABr–Glycerol.** The uptake  $\gamma_{\text{Cl}_2(t_{\text{exp}})}$  represents the fraction of incident  $\text{Cl}_2$  molecules that do not desorb within the exposure time  $t_{\text{exp}}$ . As described in ref 27,  $\gamma_{\text{Cl}_2(t_{\text{exp}})}$  can be determined by comparing the flux of  $\text{Cl}_2$  reflected from salty glycerol ( $J_{\text{Cl}_2}^{\text{soln}}$ ) to the flux reflected from pure glycerol ( $J_{\text{Cl}_2}^{\text{pure}}$ ), which does not react with  $\text{Cl}_2$ :

$$\gamma_{\text{Cl}_2(t_{\text{exp}})} = 1 - \frac{J_{\text{Cl}_2}^{\text{soln}}}{J_{\text{Cl}_2}^{\text{pure}}} \quad (1)$$

Any decrease in intensity when comparing THABr–glycerol to pure glycerol is caused by  $\text{Cl}_2$  molecules that react with  $\text{Br}^-$  or that remain dissolved over  $t_{\text{exp}}$  from  $0.047\text{s}$  to  $0.47\ \text{s}$ . (Loss by dissolution alone is negligible over these long times because  $\text{Cl}_2$  itself dissolves on average for microseconds or less in hydrocarbon and protic liquids, as discussed in ref 39.)

The uptake is measured by recording postchopper TOF spectra, shown in Figure 4, at an exit angle of  $45^\circ$  and an

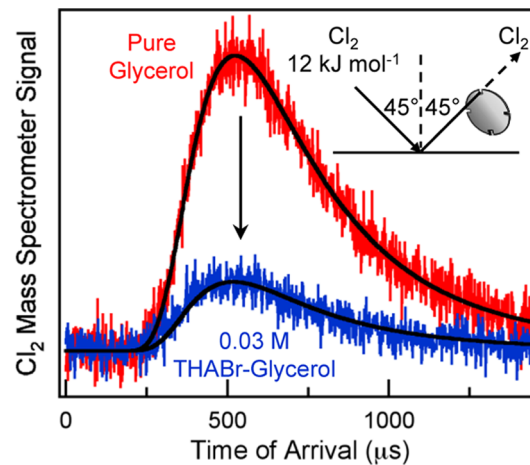


**Figure 4.** Postchopper spectra of  $12\ \text{kJ mol}^{-1}$   $\text{Cl}_2$  scattering from pure glycerol (red) and  $0.03\ \text{M}$  THABr–glycerol (blue). The black lines are MB distributions at  $290\ \text{K}$ .

incident beam energy of  $12\ \text{kJ mol}^{-1}$ . At these low collision energies ( $5RT_{\text{liq}}$ ), nearly all  $\text{Cl}_2$  molecules thermalize on the surface of the solution before they dissolve, react, or desorb. Because of the observed thermal accommodation, we assume that the ratio of fluxes at  $45^\circ$  is equal to the ratio of fluxes integrated over all exit angles,<sup>27</sup> and that  $\text{Cl}_2$  desorbs with the

same (likely cosine) angular distribution from pure glycerol and THABr-glycerol.

The measurements reveal that  $\gamma(\text{Cl}_2)$  is  $0.79 \pm 0.02$  (90% confidence interval for six measurements) in 0.03 M THABr-glycerol. This uptake is three times greater than the  $0.24 \pm 0.03$  uptake measured in 3 M NaBr-glycerol<sup>27</sup> even though both solutions have similar surface Br<sup>-</sup> concentrations of  $(7\text{--}8) \times 10^{13} \text{ cm}^{-2}$ .<sup>11</sup> The uptake in 0.03 M THABr-glycerol does not vary outside the  $\pm 0.02$  level of uncertainty when  $t_{\text{exp}}$  is stepped from 0.047 to 0.47 s, indicating that nonreacting Cl<sub>2</sub> molecules desorb over times shorter than 0.047 s. This desorption time is determined below to occur on the microsecond or shorter time scale.

### Identification and Branching Fractions of BrCl and Br<sub>2</sub> Products

As shown in Figure 5, BrCl and Br<sub>2</sub> products were detected in postchopper mode when the THABr-glycerol

solution was exposed to Cl<sub>2</sub>. Panel 5a reveals that the Br<sub>2</sub> signal dominates over the nonreactive Cl<sub>2</sub> desorption signal when using low-energy Cl<sub>2</sub> ( $E_{\text{inc}} = 12 \text{ kJ mol}^{-1}$ ), in accord with the high Cl<sub>2</sub> reactivity ( $\gamma = 0.79$ ). The TOF spectra for both species are well fit by MB distributions, indicating that Cl<sub>2</sub> dissipates its excess energy before desorbing and that Br<sub>2</sub> is not produced in direct, single-bounce collisions. A higher-flux Cl<sub>2</sub> beam was used to detect the weak BrCl signal, shown in panel 5b along with the Cl<sub>2</sub> and Br<sub>2</sub> TOF spectra. The BrCl signal is magnified 25-fold in panel 5c, revealing that the spectrum is well fit by a MB distribution.

The BrCl and Br<sub>2</sub> branching fractions may be calculated from the signal fluxes after they are corrected for the isotopic Br and Cl abundances, the partial ionization cross sections for creation of BrCl<sup>+</sup> and Br<sub>2</sub><sup>+</sup>, and the transmission function of the mass spectrometer at each ion mass. These correction factors, described in ref 27, lead to relative product fluxes of  $0.018 \pm 0.002$  for BrCl and  $0.982 \pm 0.002$  for Br<sub>2</sub> (90% confidence interval for six measurements) when the solution is exposed to the vacuum chamber for  $t_{\text{exp}} = 0.12$  s. This ratio is slightly lower than the 0.04:0.96 BrCl/Br<sub>2</sub> ratio measured under similar conditions for Cl<sub>2</sub> collisions with 3 M NaBr-glycerol.<sup>27</sup> The time scales for Cl<sub>2</sub>, BrCl, and Br<sub>2</sub> solvation and reaction are investigated in the next section by comparing pre- and postchopper spectra.

**Cl<sub>2</sub> Residence Times in Solution.** The prechopper technique can be used to determine the characteristic residence time of Cl<sub>2</sub> in solution before it escapes or reacts to form Cl<sub>2</sub>Br.<sup>27</sup> Over the duration of the  $80 \mu\text{s}$  gas pulse, shown in the “beam-on” region in Figure 6a, the desorption profile of a nonreactive atom or molecule is given by  $p_{\text{des}}(t) = 1 - \exp(t/\tau) \text{ erfc}(t/\tau)^{1/2}$ , where  $\tau$  is a characteristic bulk-phase residence time. In the “beam-off” region in panel 6a,  $p_{\text{des}}$  is determined by numerically solving the diffusion equation for absorption/desorption.<sup>27,40</sup> In both regions,  $p_{\text{des}}$  is a function of  $\tau$ , which is the time required for  $p_{\text{des}}$  to reach 57% of its maximum value:<sup>40</sup>

$$\tau = D \left( \frac{4HRT}{\beta \langle v \rangle} \right)^2 \quad (2)$$

In this expression,  $D$  is the solution-phase Cl<sub>2</sub> diffusion coefficient,  $H$  is its solubility in  $\text{M atm}^{-1}$ ,  $\beta$  is the fraction of impinging Cl<sub>2</sub> that enter solution as a neutral molecule or as Cl<sub>2</sub>Br after interfacial reaction, and  $\langle v \rangle = (8kT/\pi m)^{1/2}$  is the average thermal velocity of Cl<sub>2</sub>. Figure 6a illustrates two sample desorption profiles for  $\tau = 0$  and  $5 \mu\text{s}$  residence times. The  $\tau = 0$  profile is a square pulse because the Cl<sub>2</sub> molecules spend no time in contact with the liquid. In contrast, the  $5 \mu\text{s}$  curve shows that even pulses that are 16 times as long as  $\tau$  do not reach saturation over the pulse duration; in this case, some molecules diffuse deeply and do not evaporate for many  $\tau$  periods. Convolving  $p_{\text{des}}$  with a MB distribution simulates the shape and intensity of the Cl<sub>2</sub> prechopper TOF spectrum, as discussed below.

The measured Cl<sub>2</sub> pre- and postchopper spectra in Figure 6b were recorded following collisions of  $\sim 100 \text{ kJ mol}^{-1}$  Cl<sub>2</sub> with 0.03 M THABr-glycerol. When normalized by the IS peak intensity, the two spectra are nearly identical in shape. The IS components have been removed in panel 6c for easier comparison of the Cl<sub>2</sub> thermal desorption signals. The noise in the prechopper signal falls between the  $\tau = 0$  and  $5 \mu\text{s}$  simulations from Figure 6a, indicating that the characteristic residence time is in the microsecond regime. The maximum

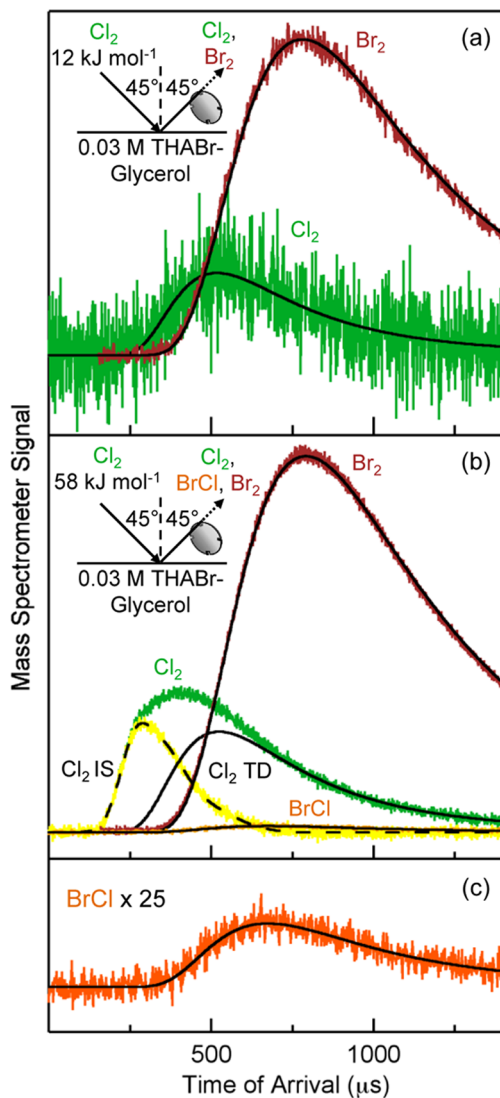


**Figure 5.** (a) Postchopper spectra of Br<sub>2</sub> (red) and Cl<sub>2</sub> (green) following collisions of  $12 \text{ kJ mol}^{-1}$  Cl<sub>2</sub> with 0.03 M THABr-glycerol. (b) Postchopper spectra of Br<sub>2</sub> (red), Cl<sub>2</sub> (green), and BrCl (orange) following collisions of  $58 \text{ kJ mol}^{-1}$  Cl<sub>2</sub> with 0.03 M THABr-glycerol. The IS component of the high-energy Cl<sub>2</sub> scattering is shown in yellow. (c) The BrCl signal from panel 5b magnified 25-fold. The solid black lines in all panels are MB distributions at 290 K, and the exposure time  $t_{\text{exp}}$  for all spectra is 0.12 s.

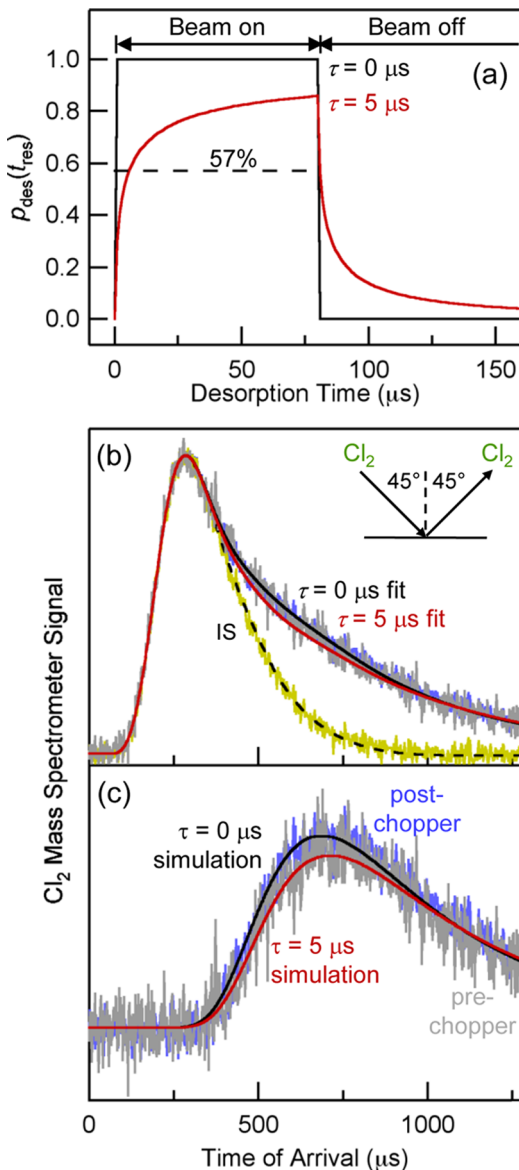


**Figure 6.** (a) Desorption probabilities  $p_{\text{des}}$  for  $\tau = 0 \mu\text{s}$  (black) and  $5 \mu\text{s}$  (red). At time  $\tau$ , the desorption flux reaches 57% of its maximum value, as indicated by the dashed line. The durations of the beam-on and beam-off regions are  $80 \mu\text{s}$  and  $3.92 \text{ ms}$ , respectively. (b) Postchopper (blue) and prechopper (gray) spectra measured from  $\sim 100 \text{ kJ mol}^{-1}$   $\text{Cl}_2$  scattering from  $0.03 \text{ M}$  THABr-glycerol. The postchopper IS component is shown in yellow. (c) TD component extracted from the  $\text{Cl}_2$  post- and prechopper spectra. The  $0 \mu\text{s}$  (black) and  $5 \mu\text{s}$  (red) simulations were generated by convolving the desorption profiles from panel 6a with a MB distribution at mass-to-charge ratio  $m/z = 70$  and  $T_{\text{liq}} = 290 \text{ K}$ . The  $0$  and  $5 \mu\text{s}$  prechopper fits in panel 6b are the sum of the dashed IS fit in panel 6b with the simulations from panel 6c.

average depth that  $\text{Cl}_2$  molecules travel into solution within  $5 \mu\text{s}$  is roughly  $0.6(D\tau)^{1/2} \approx 7 \text{ \AA}$  using  $D = 3 \times 10^{-9} \text{ cm}^2 \text{ s}^{-1}$ .<sup>27</sup> This diffusion depth is comparable to the  $\sim 5 \text{ \AA}$  size of a glycerol molecule and  $\sim 10 \text{ \AA}$  size of a  $\text{THA}^+$  ion, suggesting that most  $\text{Cl}_2$  do not penetrate deeper than 1–2 monolayers before reacting with  $\text{Br}^-$  or returning to the gas phase. These prechopper measurements are our most direct indication that  $\text{Cl}_2$  reacts rapidly in the interfacial region.<sup>41</sup>

**Br<sub>2</sub> Residence Times Following Br<sub>2</sub> Absorption.** Before measuring the more complex time for production of  $\text{Br}_2$  from  $\text{Cl}_2$ , we measured the characteristic residence time of  $\text{Br}_2$  itself in  $0.03 \text{ M}$  THABr-glycerol by exposing the solution to  $\text{Br}_2$  molecules at  $E_{\text{inc}} = 150 \text{ kJ mol}^{-1}$ . This high-energy beam was used because it enables a clear separation of the IS and TD components. Figure 7b and c displays the pre- and postchopper

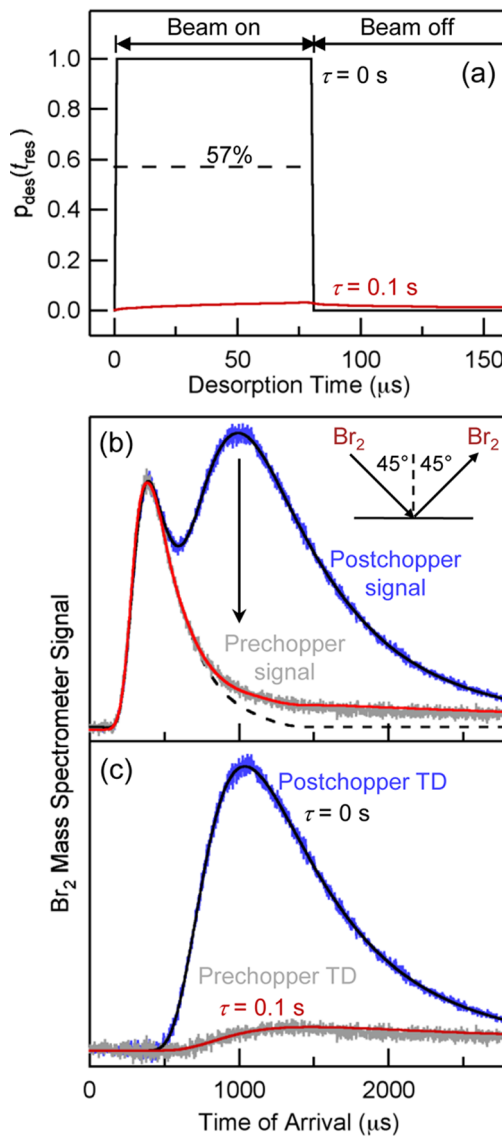


**Figure 7.** (a)  $p_{\text{des}}$  for  $\tau = 0 \text{ s}$  (black) and  $0.1 \text{ s}$  (red). The integrated areas of the desorption profiles are equal because of the long-time tail (not shown) of the  $0.1 \text{ s}$  curve. (b) Postchopper (blue) and prechopper (gray) spectra measured from collisions of  $150 \text{ kJ mol}^{-1}$   $\text{Br}_2$  with  $0.03 \text{ M}$  THABr-glycerol. The downward arrow marks the decrease in thermal desorption. (c) The TD component of the  $\text{Br}_2$  post- and prechopper spectra. See the caption from Figure 6.

spectra with and without the inelastic scattering components: the strong postchopper  $\text{Br}_2$  signal almost disappears in the prechopper spectrum, where the signal is barely visible above the baseline. This weak prechopper signal implies that nearly all  $\text{Br}_2$  molecules that enter the solution remain dissolved over the 4 ms recording time between gas pulses. The best-fit characteristic residence time is found to be  $\tau \geq 0.1 \text{ s}$  using the distribution for  $p_{\text{des}}$  in panel 7a.<sup>42</sup> This  $0.1 \text{ s}$  residence time

is  $10^5$  times longer than  $\tau(\text{Cl}_2)$  and  $10^4$  times longer than  $\tau(\text{Br}_2)$  in 3 M NaBr–glycerol (see Table 1 for a list of

**Table 1. Characteristic Residence Times for  $\text{Br}_2$  and  $\text{Cl}_2$**

glycerol solution	$\tau(\text{Br}_2)$ (s)	$\tau(\text{Cl}_2)$ (s)
pure glycerol	< $10^{-6}$	< $10^{-6}$ (ref 27)
0.03 M NaBr	$\leq 10^{-6}$	
3 M NaBr	$\sim 10^{-5}$ (ref 27)	< $10^{-6}$ (ref 27)
0.03 M TEABr	$\leq 10^{-6}$	
0.03 M THACl	$\sim 10^{-3}$	$\leq 10^{-6}$
0.03 M THABr	$\geq 10^{-1}$	$\sim 10^{-6}$
0.6 M NaCl–0.03 M THABr	$\geq 10^{-1}$	< $10^{-6}$

measured  $\text{Br}_2$  and  $\text{Cl}_2$  residence times).<sup>27</sup> Using eq 2 and  $\beta \approx 1$ , the 0.1 s value corresponds to an effective solubility for  $\text{Br}_2$  of  $10^6 \text{ M atm}^{-1}$  and a solvation free energy of  $-40 \text{ kJ mol}^{-1}$ . This  $\text{Br}_2$  solubility is  $\sim 100$  times greater than in 3 M NaBr, despite its much larger bulk-phase  $\text{Br}^-$  concentration. As discussed later, the large change in solubility is likely driven by reaction of  $\text{Br}_2$  with  $\text{Br}^-$  to produce  $\text{Br}_3^-$  ions that complex with THA<sup>+</sup> cations.

**Formation and Residence Times of  $\text{BrCl}$  and  $\text{Br}_2$  Products.** The prechopper technique was next used to measure the lifetime of  $\text{BrCl}$  and  $\text{Br}_2$  products formed by reaction when  $\text{Cl}_2$  molecules strike the surface of THABr–glycerol. The differences between the pre- and postchopper TOF spectra depend on the reaction times for converting  $\text{Cl}_2$  to  $\text{BrCl}$  and  $\text{Br}_2$  and for solvation and diffusion of the intermediates and products prior to desorption. The  $\text{BrCl}$  pre- and postchopper spectra in Figure 8a have identical shapes within the level of noise, indicating that the only  $\text{BrCl}$

molecules that desorb are those produced from decomposition of  $\text{Cl}_2\text{Br}^-$  close to the surface and within a few microseconds. This short time is in accord with the  $\sim 10 \mu\text{s}$   $\text{BrCl}$  lifetime measured in 3 M NaBr–glycerol.<sup>27</sup>

In contrast, the  $\text{Br}_2$  product originating from  $\text{Cl}_2$  has such a long lifetime in 0.03 M THABr that the prechopper signal in Figure 8b is almost indiscernible above the baseline. This prechopper spectrum is even slightly flatter than the spectrum in Figure 7c for collisions of  $\text{Br}_2$  with 0.03 M THABr. The shape of the prechopper simulations for  $\tau > 10^{-1} \text{ s}$  does not vary enough for us to quantify this difference precisely, and we can only say that the delay time for producing  $\text{Br}_2(\text{g})$  from  $\text{Cl}_2(\text{g})$  exceeds 0.1 s. We do know that any additional time in forming  $\text{Br}_2$  from  $\text{Cl}_2$  cannot arise from the lifetime of the  $\text{Br}_2\text{Cl}^-$  intermediate, shown in Figure 1; this lifetime was measured from collisions of  $\text{Br}_2$  with 0.03 M THACl to be only  $10^{-3} \text{ s}$  (Table 1). The weak prechopper spectra in both Figures 7c and 8b lead us to conclude that the long residence times ( $\tau \geq 0.1 \text{ s}$ ) likely arise from the enhanced solubility of  $\text{Br}_2$  because of formation of  $\text{THA}^+\text{Br}_3^-$ .

**Reaction in Mixed Chloride/Bromide Solution.** We prepared a mixed solution of 0.6 M NaCl and 0.03 M THABr in glycerol to investigate halogen exchange when  $\text{Cl}^-$  outnumbers  $\text{Br}^-$  by 20:1 in the bulk. The net uptake of  $\text{Cl}_2$  into this mixed solution remains high despite the large stoichiometric excess of  $\text{Cl}^-$  ions: as shown in Figure 9a,  $\gamma = 0.46 \pm 0.01$  (90% confidence interval for three measurements), which falls in between the  $0.24 \pm 0.03$   $\text{Cl}_2$  uptake into 3 M NaBr<sup>27</sup> and the  $0.79 \pm 0.02$  uptake into 0.03 M THABr. Both  $\text{BrCl}$  and  $\text{Br}_2$  are produced in the mixed solution, as shown in Figure 9b for collisions of  $58 \text{ kJ mol}^{-1} \text{ Cl}_2$ . The postchopper spectra indicate that the  $\text{BrCl}$  and  $\text{Br}_2$  branching fractions are  $7.1 \pm 0.5\%$  and  $92.9 \pm 0.5\%$  (90% confidence interval for six measurements). This 7%  $\text{BrCl}$  fraction exceeds the fractions in the chloride-free solutions of 0.03 M THABr and 3 M NaBr by at least 7-fold.

The time scales for  $\text{Cl}_2$  capture and  $\text{BrCl}$  and  $\text{Br}_2$  production were then measured by comparing the pre- and postchopper spectra of each species. Because the  $\text{Cl}_2$  pre- and postchopper spectra (not shown) have identical intensities and shapes within the noise level, we conclude that  $\text{Cl}_2$  capture in NaCl–THABr–glycerol occurs on a microsecond or shorter time scale. This result is in accord with the  $<5 \mu\text{s}$  residence time of  $\text{Cl}_2$  in 0.03 M THABr and the  $<1 \mu\text{s}$  residence time in 3 M NaBr.

Preliminary results from prechopper experiments suggest that the reaction kinetics following halogen capture are more complex in the NaCl–THABr solution than in 0.03 M THABr or 3 M NaBr. Whereas  $\text{BrCl}$  molecules rapidly desorb from the near-interfacial regions in the chloride-free solutions, hundreds of microseconds elapse before they desorb from the mixed NaCl–THABr solution. With reference to Figure 1, this long delay and the enhanced 7% escape of  $\text{BrCl}$  may be due to excess  $\text{Cl}^-$  ions that reduce the interfacial concentration of  $\text{Br}^-$  and slow the destruction of  $\text{BrCl}$  by  $\text{Br}^-$  into  $\text{Br}_2\text{Cl}^-$ .  $\text{Br}_2$  exhibits a comparable 0.1 s or greater lifetime in the NaCl–THABr and THABr solutions, implying that the lifetime of  $\text{Br}_2$  is controlled by its equilibrium with  $\text{Br}_3^-$  even in the presence of excess  $\text{Cl}^-$ .

**Evidence for Saturation of THA<sup>+</sup>/Br<sup>−</sup> Surface Sites by  $\text{Cl}_2$ .** We observed a surprising change in signal when comparing the scattering of 12 and  $58 \text{ kJ mol}^{-1} \text{ Cl}_2$  molecules as a function of  $t_{\text{exp}}$ . As mentioned earlier, there was no dependence of  $\gamma(\text{Cl}_2)$

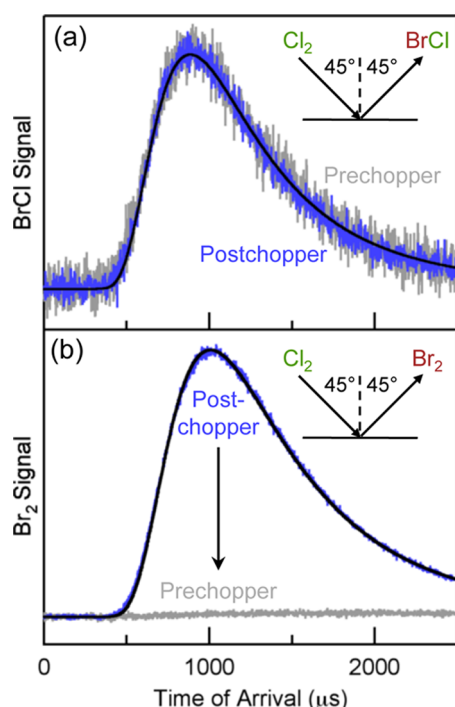


**Figure 8.** Postchopper (blue) and prechopper (gray) spectra for (a)  $\text{BrCl}$  and (b)  $\text{Br}_2$  following collisions of  $58 \text{ kJ mol}^{-1} \text{ Cl}_2$  with 0.03 M THABr–glycerol. The black lines through the postchopper spectra are MB distributions at 290 K. The post- and prechopper spectra in panel 8a are peak-normalized to compare their shapes.

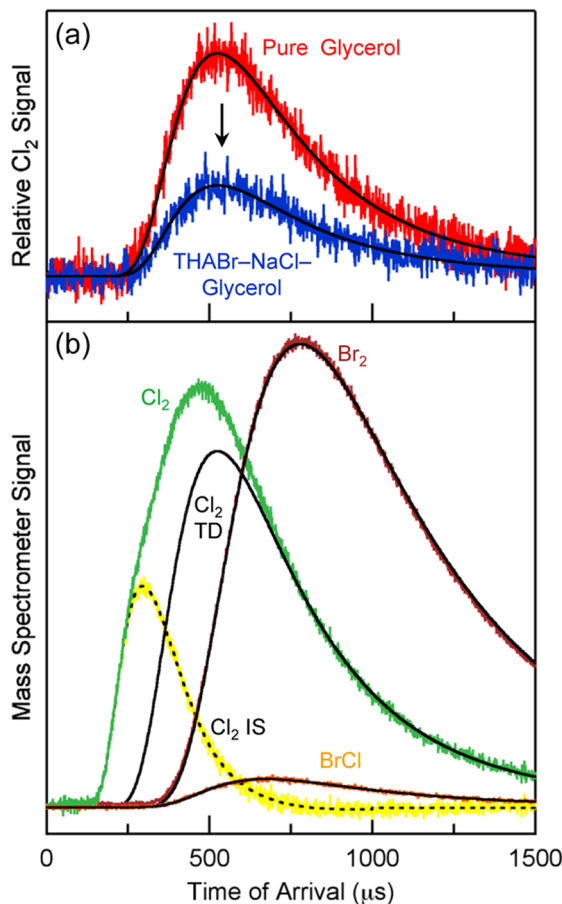


**Figure 9.** (a) Postchopper spectra of  $12 \text{ kJ mol}^{-1}$   $\text{Cl}_2$  scattering from pure glycerol (red) and 0.6 M NaCl–0.03 M THABr–glycerol (blue). (b) Postchopper spectra of  $\text{Br}_2$  (red),  $\text{Cl}_2$  (green), and  $\text{BrCl}$  (orange) following collisions of  $58 \text{ kJ mol}^{-1}$   $\text{Cl}_2$  with 0.6 M NaCl–0.03 M THABr–glycerol for  $t_{\text{exp}} = 0.12 \text{ s}$ . The IS component of the  $\text{Cl}_2$  spectrum is shown in yellow. The solid black lines are MB distributions at 290 K.

on exposure time when scattering  $12 \text{ kJ mol}^{-1}$   $\text{Cl}_2$  from 0.03 M THABr–glycerol, but Figure 10 shows that the  $\text{Cl}_2$  thermal

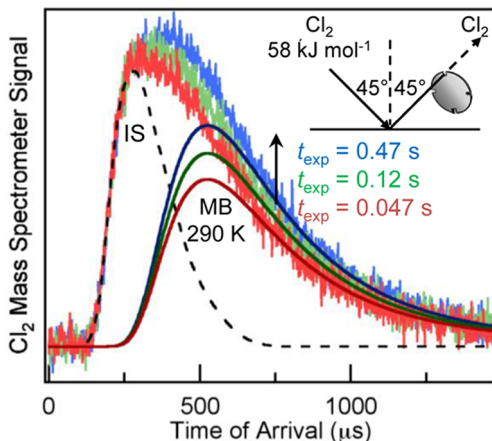


**Figure 10.** Postchopper spectra of  $58 \text{ kJ mol}^{-1}$   $\text{Cl}_2$  scattering from 0.03 M THABr–glycerol at  $t_{\text{exp}} = 0.047 \text{ s}$  (red),  $0.12 \text{ s}$  (green), and  $0.47 \text{ s}$  (blue). The dashed line is a fit to the IS component, and the solid lines are MB distributions at 290 K.

desorption signal increases by  $23 \pm 2\%$  (two measurements) when  $t_{\text{exp}}$  is increased from  $0.047$  to  $0.47 \text{ s}$  at  $E_{\text{inc}} = 58 \text{ kJ mol}^{-1}$ . The increase in  $\text{Cl}_2$  desorption with exposure time is analyzed in the Appendix: we think it is best explained by saturation of  $\text{THA}^+$  surface sites when exposed for long times to the  $58 \text{ kJ mol}^{-1}$   $\text{Cl}_2$  beam, which is  $\sim 9$  times higher in flux than the  $12 \text{ kJ mol}^{-1}$  beam. If this interpretation is correct, it implies that even reaction sites at the surface of a liquid can be saturated by an impinging gas if these sites are replenished more slowly than their reaction with gas-phase molecules.

## DISCUSSION

The experiments reveal two key findings. First, 79% of the  $\text{Cl}_2$  molecules impinging on the surface of 0.03 M THABr–glycerol react to produce  $\text{BrCl}$  and  $\text{Br}_2$ . This reactivity is three times higher than the 24% value measured for 3 M NaBr–glycerol<sup>27</sup> even though the two solutions have comparable  $\text{Br}^-$  surface coverages [ $(7\text{--}8) \times 10^{13} \text{ cm}^{-2}$  determined from their adsorption isotherms<sup>11</sup>]. Second,  $\text{THA}^+$  ions at only 0.03 M concentration lengthen the solvation time of  $\text{Br}_2/\text{Br}_3^-$  by at least  $10^4$  in comparison to a 3 M  $\text{Na}^+$  solution. We postulate that  $\text{THA}^+$  ions promote both enhancements by creating charged, solvent-excluding pockets that preferentially associate with large anions. As pictured in Figure 1, these pockets provide a local environment in which  $\text{Cl}_2$  and  $\text{Br}_2$  react with  $\text{Br}^-$  to form  $\text{Cl}_2\text{Br}^-$  and  $\text{Br}_3^-$ , respectively.

**Interfacial Capture of  $\text{Cl}_2$  by  $\text{THA}^+$ .** The motivation for the picture in Figure 1 arises from simulations of tetraalkylammonium halides in water by Jungwirth and co-workers.<sup>10,43</sup> Figure 11a, for example, shows that the

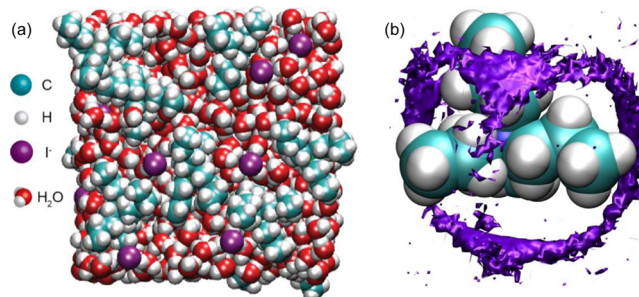


**Figure 11.** (a) Molecular dynamics snapshot of 1 M tetrabutylammonium iodide (TBAI) in water as seen from the top. Reprinted with permission from ref 10. Copyright 2004 American Chemical Society. (b) Distribution of  $\text{I}^-$  about the tetrapropylammonium (TPA<sup>+</sup>) cation in a 1 M aqueous solution. The probability density indicated in purple is 10 times greater than the bulk density. Simulation provided by Jan Heyda and Pavel Jungwirth.

tetrabutylammonium ion ( $\text{TBA}^+$ ) is asymmetrically solvated at the surface, exposing a partially bare charge to vacuum that could preferentially interact with  $\text{Cl}_2$  and  $\text{Cl}_2\text{Br}^-$ . The  $\text{I}^-$  counterions in the simulation reside just below or within the surface layer. On the surface itself,  $\text{TBA}^+$  is preferentially oriented to minimize unfavorable interactions between the hydrophobic alkyl chains and the polar liquid: three of the hydrocarbon chains are aligned in the plane of the surface, and the remaining chain is directed into the liquid.<sup>10,12</sup> This predicted orientation is consistent with experiments by Morgner and co-workers for  $\text{TBA}^+$  at the surface of formamide,<sup>12</sup> and we therefore assume that  $\text{THA}^+$  on glycerol behaves in a similar way. Further experiments involving TBAI

suggest that  $\text{TBA}^+$  draws  $\text{I}^-$  to the outermost layers in solutions of formamide,<sup>19,44</sup> and separate studies indicate that  $\text{Br}^-$  ions also populate the surface region of water.<sup>15,18,45,46</sup> For THABr, the  $\text{Br}^-$  ions must be located close to the  $\text{THA}^+$  ions in order to preserve charge neutrality. Together, these studies suggest that  $\text{Br}^-$  is present just below or within the surface layer of  $\text{THA}^+$  ions in THABr–glycerol.

Our experiments do not reveal the relative timing of the interactions among  $\text{Cl}_2$ ,  $\text{Br}^-$ , and  $\text{THA}^+$ , but Figure 1 presents one possible scenario. In this picture,  $\text{THA}^+$  ions in the interfacial region interact preferentially with thermally accommodated  $\text{Cl}_2$  molecules through attractions between  $\text{Cl}_2$  and both the hexyl chains and the charge of the exposed  $\text{THA}^+$  ion. These interactions draw the  $\text{Cl}_2$  molecules into contact with nearby  $\text{Br}^-$  ions at or below the surface. As a result,  $\text{Cl}_2$  molecules require fewer contacts with the surface to react in 0.03 M THABr when compared to 3 M NaBr–glycerol, where both  $\text{Na}^+$  and  $\text{Br}^-$  are likely to be better solvated, perhaps buried in valleys formed by surface glycerol molecules.<sup>19</sup> We previously estimated that the lifetime of  $\text{Cl}_2$  at the surface of the 3 M NaBr solution is roughly 50 ps and, by comparison with simulations of OH collisions with a 1.2 M NaI–water solution, that ~1 in 30 contacts with  $\text{Br}^-$  leads to  $\text{Cl}_2\text{Br}^-$  formation.<sup>27</sup> The substitution of  $\text{THA}^+$  for  $\text{Na}^+$  enhances  $\text{Cl}_2$  reactivity 3-fold, such that reaction may occur within only ~10 contacts with interfacial  $\text{Br}^-$ .

**Formation of  $\text{Br}_3^-$  and Complexation with  $\text{THA}^+$ .** Table 1 lists  $\text{Br}_2$  and  $\text{Cl}_2$  residence times measured in glycerol solutions of various salts and surfactants. They illustrate that both the anion and cation control the lifetimes of  $\text{Br}_2$  in glycerol, while they do not measurably alter the lifetimes of  $\text{Cl}_2$ . The enhancement by dissolved  $\text{Br}^-$  most likely arises from the reversible reaction  $\text{Br}_2(\text{g}) + \text{Br}^-(\text{gly}) \leftrightarrow \text{Br}_3^-(\text{gly})$  and perhaps formation of  $\text{Br}_5^-$  and higher polybromides, with analogous equilibria for other trihalide species.<sup>27,47</sup> These equilibria increase the lifetime of  $\text{Br}_2$  in glycerol from less than  $10^{-6}$  s in pure glycerol to  $10^{-3}$  s in 0.03 M THACl and to  $10^{-1}$  s in 0.03 M THABr (Table 1). The trends are in accord with the stabilities of  $\text{Br}_3^-$ ,  $\text{Br}_2\text{Cl}^-$ , and  $\text{Cl}_3^-$  in water: the equilibrium constants for these trihalide species are  $12 \text{ atm}^{-1}$  for  $\text{Br}_2(\text{g}) + \text{Br}^-(\text{aq}) \leftrightarrow \text{Br}_3^-(\text{aq})$ , 1.0 for  $\text{Br}_2(\text{g}) + \text{Cl}^-(\text{aq}) \leftrightarrow \text{Br}_2\text{Cl}^-(\text{aq})$  and only 0.017 for  $\text{Cl}_2(\text{g}) + \text{Cl}^-(\text{aq}) \leftrightarrow \text{Cl}_3^-(\text{aq})$ .<sup>47,48</sup> The much smaller value for the last reaction implies that  $\text{Cl}_3^-$  should not be a sink for  $\text{Cl}_2$  in glycerol, as confirmed by its submicrosecond residence times in both THACl and NaCl–THABr.

These comparisons may be made quantitative for the  $\text{Br}_2$  lifetimes in 3 M NaBr ( $\tau \approx 10 \mu\text{s}$ ) and in 0.03 M THABr ( $\tau \geq 0.1$  s) by calculating the effective  $\text{Br}_2$  solubility  $H^*$  using eq 2, which shows that  $\tau$  scales as  $H^{*2}$ . The  $10^4$ -fold ratio of residence times for the two solutions indicates that  $\text{Br}_2$  is ~100 times more soluble in 0.03 M THABr than in 3 M NaBr, despite the 100-fold lower  $\text{Br}^-$  concentration. To gain more insight, we can recast eq 2 in terms of  $[\text{Br}^-]$  and the equilibrium constant  $K$  for  $\text{Br}_2(\text{g}) + \text{Br}^-(\text{gly}) \leftrightarrow \text{Br}_3^-(\text{gly})$ . This rearrangement yields  $\tau = D(4RTK[\text{Br}^-]/\beta\langle v \rangle)^2$ , showing that  $\tau$  scales with  $(K[\text{Br}^-])^2$  when the activity coefficient ratio  $f(\text{Br}_3^-)/f(\text{Br}^-)$  is close to one. The  $10^4$ -fold ratio in residence times implies that the equilibrium constant  $K$  for  $\text{Br}_2(\text{g}) + \text{THA}^+\text{Br}^- \leftrightarrow \text{THA}^+\text{Br}_3^-$  is also  $10^4$  times greater than  $K$  for the analogous reaction when  $\text{Na}^+$  is substituted for  $\text{THA}^+$ .

This enormous shift toward  $\text{Br}_3^-$  suggests that  $\text{THA}^+\text{Br}_3^-$  could be considered as a distinct and stable species in glycerol,

with  $\text{Br}_3^-$  stabilized by the  $\text{THA}^+$  ion to survive for at least 0.1 s.<sup>49</sup> We emphasize that this tight ion pairing does not exist for the smaller species TEA<sup>+</sup>,  $\text{N}(\text{CH}_3\text{CH}_2)_4\text{Br}$ , whose lifetime is short ( $\tau \leq 10^{-6}$  s). This comparison indicates that the alkyl chains of the  $\text{TAA}^+$  ion must be longer than  $\text{CH}_3\text{CH}_2$  to create a local hydrophobic environment that stabilizes  $\text{Br}_3^-$  and enables  $\text{TAA}^+$  and  $\text{Br}_3^-$  to form a long-lived complex. The  $10^{-3}$  s residence time measured for  $\text{THA}^+\text{Br}_2\text{Cl}^-$  implies that this complex may also be strongly bound and further suggests that the residence time of  $\text{Cl}_2\text{Br}^-$ , although below the  $10^{-6}$  s detection limit in our experiments, may also be enhanced by  $\text{THA}^+$  over  $\text{Na}^+$ .

Within the pictures presented above, it is intriguing to speculate that the enhancement in  $\text{Br}_2$  solubility and increase in  $\text{Cl}_2$  reactivity from 3 M NaBr to 0.03 M THABr share a common origin in the stabilization of the  $\text{THA}^+\text{Br}_3^-$  and  $\text{THA}^+\text{Cl}_2\text{Br}^-$  complexes, rendered especially favorable by the large sizes and diffuse charge densities of the ions.<sup>43,50,51</sup> Recent simulations provide theoretical support for strong interactions between ions of similar size:<sup>43</sup> Figure 11b, generated by Heyda and Jungwirth, shows that the probability density of  $\text{I}^-$  is enhanced at least 10-fold in the vicinity of the tetrapropylammonium ion ( $\text{TPA}^+$ ) with respect to the bulk solution. In the larger  $\text{THA}^+\text{Cl}_2\text{Br}^-$  and  $\text{THA}^+\text{Br}_3^-$  complexes, the  $\text{Cl}_2\text{Br}^-$  and  $\text{Br}_3^-$  ions are likely to be attracted toward the first few  $\text{CH}_2$  groups, where the positive charge is broadly distributed on  $\text{THA}^+$ . In particular, very little charge is calculated to reside on the central N atom, only +0.003 in  $\text{TPA}^+$ , in comparison to charges of +0.07, 0.03, and 0.05 on the H atoms of the C<sub>1</sub>, C<sub>2</sub>, and C<sub>3</sub> methylene groups of each chain.<sup>43</sup> The dispersed charge on  $\text{THA}^+$  is particularly well suited to stabilize the dispersed charge on  $\text{Br}_3^-$ , which is distributed among the terminal Br atoms (~42%) and the inner Br atom (16%).<sup>52</sup> Further evidence for local  $\text{THA}^+\text{Br}_3^-$  interactions comes from simulations of  $\text{TBA}^+\text{Cl}^-$  ion pairing<sup>13</sup> and from the crystal structure determination of  $\text{TBA}\text{Br}_3$ ,<sup>53</sup> which reveal that  $\text{Cl}^-$  and the linear  $\text{Br}_3^-$  ion intercalate between the butyl chains of  $\text{TBA}^+$ . Similar interactions with  $\text{THA}^+$  may also stabilize the more localized charge on  $\text{Cl}\text{Cl}\text{Br}^-$  and even attract neutral  $\text{Cl}_2$  molecules between the chains via ion-induced dipole forces, perhaps increasing the opportunities for reaction with neighboring  $\text{Br}^-$ .

**$\text{Cl}_2 + \text{Br}^-$  Reactions in Excess  $\text{Cl}^-$ .** The 0.6 M NaCl/0.03 M THABr mixture illustrates the power of ionic surfactants such as  $\text{THA}^+$  to catalyze the conversion of  $\text{Cl}_2$  into  $\text{BrCl}$  and  $\text{Br}_2$  even when  $\text{Cl}^-$  outnumbers  $\text{Br}^-$  by 20:1. At such high ratios, the  $\text{Cl}^-$  ions may crowd some interfacial  $\text{Br}^-$  ions into the bulk, despite the greater propensity of  $\text{Br}^-$  than  $\text{Cl}^-$  to segregate to the surface region.<sup>18</sup> We do not know the  $\text{Br}^-$  and  $\text{Cl}^-$  ion surface concentrations for this mixture, but Winter and co-workers observed only a modest crowding of  $\text{I}^-$  by  $\text{Br}^-$  when adding 1 m NaBr to 0.02 m TBAI in water, where they found that the interfacial  $\text{I}^-$  concentration dropped by 60% upon adding excess NaBr.<sup>54</sup> In our less extreme case in which the  $\text{Cl}^-/\text{Br}^-$  ratio is 20:1, the  $\text{Cl}_2$  reaction probability is measured to be 46%, a drop of less than half from the 79% reactivity in the absence of  $\text{Cl}^-$  and still almost double the 24% reactivity of the 3 M NaBr solution. These comparisons suggest that high bulk concentrations of  $\text{Cl}^-$  ions do not effectively expel  $\text{Br}^-$  from the interfacial region of glycerol, at least in the presence of  $\text{THA}^+$ , and that surface  $\text{THA}^+$  still enhances the reaction of  $\text{Br}^-$  with thermally equilibrated  $\text{Cl}_2$  at the surface of the solution.

## CONCLUSIONS

The high 79%  $\text{Cl}_2$  uptake into 0.03 M THABr–glycerol underscores the power of ionic surfactants to catalyze interfacial reactions and transport species across the gas–liquid interface. It appears that surface  $\text{THA}^+$  ions “tease” impinging  $\text{Cl}_2$  molecules into solution: the surfactant provides a charged, hydrophobic environment for solvation and reaction with  $\text{Br}^-$ , which occurs on a microsecond or shorter time scale and within the top few monolayers of solution. Flux-dependent deposition studies further reveal that uncomplexed  $\text{THA}^+$  must be available at the surface for  $\text{Cl}_2$  entry to occur. The propensity of  $\text{THA}^+$  to form complexes with trihalide anions also controls the remarkably high solubility of  $\text{Br}_2$  in THABr–glycerol: incident  $\text{Br}_2$  molecules remain dissolved in solution for extremely long times ( $\tau \geq 0.1$  s) because  $\text{THA}^+$  stabilizes the  $\text{Br}_3^-$  anions formed from  $\text{Br}_2$  and  $\text{Br}^-$ . We find that the length of the alkyl chain matters, as the substitution of  $\text{TEA}^+$  for  $\text{THA}^+$  reduces the  $\text{Br}_2$  lifetime to  $\leq 1\ \mu\text{s}$ . Additionally,  $\text{THA}^+$  enhances  $\text{Cl}_2$  conversion to  $\text{Br}_2$  even when the THABr solution is doped with a 20-fold excess of  $\text{NaCl}$ , perhaps because  $\text{THA}^+$  pairs preferentially with the larger  $\text{Br}^-$  ion.

These experiments challenge the expectation that bulky surfactants must block gas uptake and impede reactions.<sup>1,6,9,55,56</sup> At a bulk concentration of 0.03 M, THABr reaches an approximate surface coverage of only 50%. This packing of  $\text{THA}^+$  ions is not tight enough to significantly prohibit solute transport through the interfacial region, which also contains the  $\text{Br}^-$  reactant. Instead, the  $\text{THA}^+$  ions appear to provide a charged and hydrophobic environment that promotes reaction by bringing together gas-phase and solution-phase reactants at the surface. It may even be possible that similar cationic surfactants in sea spray draw gaseous  $\text{Cl}_2$  and  $\text{Br}^-$  ions together at the surface to generate  $\text{Br}_2$ . The experiments here suggest that  $\text{Cl}_2 \rightarrow \text{Br}_2$  turnover is high: of the  $\text{Cl}_2$  molecules striking the surface of THABr–glycerol, 77% are converted to  $\text{Br}_2$  in the absence of  $\text{NaCl}$  and 43% in the presence of a 20-fold  $\text{Cl}^-$  excess. We hope in future experiments to extend these halogen exchange studies to aqueous seawater itself using the liquid microjet technique.<sup>57</sup>

## APPENDIX: SATURATION OF SURFACE REACTION SITES BY IMPINGING $\text{Cl}_2$ MOLECULES

Figure 10 shows that the  $\text{Cl}_2$  signal increases by 23% over exposure times from  $t_{\exp} = 0.047$  to 0.47 s when  $E_{\text{inc}} = 58\ \text{kJ mol}^{-1}$ , yet the uptake measurements in Figure 4 from 12  $\text{kJ mol}^{-1}$   $\text{Cl}_2$  scattering are independent of  $t_{\exp}$ . We interpret the change in  $\text{Cl}_2$  desorption in Figure 10 by noting that longer exposure times also mean that a larger number of  $\text{Cl}_2$  molecules strike the same patch of surface on the coated wheel. More  $\text{Cl}_2$  molecules will then desorb at longer  $t_{\exp}$  because there are not enough interfacial  $\text{Br}^-$  and  $\text{THA}^+$  ions to react with the greater number of impinging  $\text{Cl}_2$ : diffusion from below is too slow to replace the surface  $\text{THA}^+$  and  $\text{Br}^-$  ions that are already tied up by binding to  $\text{Cl}_2$ .

The  $\text{Cl}_2$  saturation flux can be estimated by calculating the number of  $\text{THA}^+$  and  $\text{Br}^-$  ions accessible to  $\text{Cl}_2$  over the maximum 0.47 s exposure time. The 0.03 M THABr solution generates a surface layer of  $\text{THA}^+$  and  $\text{Br}^-$  ions at a concentration of  $\sim 8 \times 10^{13}\ \text{cm}^{-2}$ .<sup>11</sup> This layer is continuously replenished by diffusive exchange with subsurface ions. Assuming a diffusion constant of  $\sim 10^{-9}\ \text{cm}^2\ \text{s}^{-1}$ ,  $\text{THA}^+$  and  $\text{Br}^-$  ions diffuse through a depth of  $\sim 2000\ \text{\AA}$  over 0.5 s. For a

0.03 M solution, the  $\text{THA}^+$  and  $\text{Br}^-$  concentrations over this depth are each  $\sim 4 \times 10^{14}\ \text{cm}^{-2}$ , which predict that  $\sim 5 \times 10^{14}\ \text{cm}^{-2}$  are available for each ion when including the surface monolayer.  $\text{Cl}_2$  will react with these  $\text{Br}^-$  and  $\text{THA}^+$  ions in 0.47 s for beam fluxes greater than  $10^{15}\ \text{cm}^{-2}\ \text{s}^{-1}$ .

The fluxes of the  $\text{Cl}_2$  beams were not directly measured in these experiments, but a value of  $\sim 10^{15}\ \text{cm}^{-2}\ \text{s}^{-1}$  for the 58  $\text{kJ mol}^{-1}$  beam (3%  $\text{Cl}_2$  in He at 395 K) is in accord with previous flux measurements of HCl beams created under similar conditions.<sup>58</sup> We did directly verify that the 12  $\text{kJ mol}^{-1}$  beam (5%  $\text{Cl}_2$  in Ar at 395 K) was  $\sim 9$  times lower in flux than the 58  $\text{kJ mol}^{-1}$  beam, suggesting that the low-energy beam would be less effective in saturating the interfacial region; this conclusion is in accord with our observations that there was no noticeable change in  $\text{Cl}_2$  desorption with  $t_{\exp}$  when using this lower flux beam. Within this interpretation, the experiments provide an example of a natural damping mechanism for gas–liquid reactions in which the turnover of a soluble surfactant layer is slower than the gas-surface reaction rate.

## AUTHOR INFORMATION

### Corresponding Author

\*E-mail: gmnathan@wisc.edu. Telephone: 608-262-8098.

### Notes

The authors declare no competing financial interest.

## ACKNOWLEDGMENTS

This material is based upon work supported by the National Science Foundation under Grant Nos. CHE-0809681 and CHE-1152737 and by a NSF Graduate Research Fellowship to JAF under Grant No. DGE-0718123. We are grateful to NSF for funding this work and to Pavel Jungwirth for insightful discussions and for providing Figure 11.

## REFERENCES

- (1) Donaldson, D. J.; Vaida, V. The Influence of Organic Films at the Air-Aqueous Boundary on Atmospheric Processes. *Chem. Rev.* **2006**, *106*, 1445–1461.
- (2) Gilman, J. B.; Vaida, V. Permeability of Acetic Acid Through Organic Films at the Air-Aqueous Interface. *J. Phys. Chem. A* **2006**, *110*, 7581–7587.
- (3) Hayase, S.; Yabushita, A.; Kawasaki, M.; Enami, S.; Hoffmann, M. R.; Colussi, A. J. Weak Acids Enhance Halogen Activation on Atmospheric Water's Surfaces. *J. Phys. Chem. A* **2011**, *115*, 4935–4940.
- (4) Clifford, D.; Donaldson, D. J. Direct Experimental Evidence for a Heterogeneous Reaction of Ozone with Bromide at the Air-Aqueous Interface. *J. Phys. Chem. A* **2007**, *111*, 9809–9814.
- (5) Clifford, D.; Bartels-Rausch, T.; Donaldson, D. J. Suppression of Aqueous Surface Hydrolysis by Monolayers of Short Chain Organic Amphiphiles. *Phys. Chem. Chem. Phys.* **2007**, *9*, 1362–1369.
- (6) Thornton, J. A.; Abbatt, J. P. D.  $\text{N}_2\text{O}_5$  Reaction on Submicron Sea Salt Aerosol: Kinetics, Products, and the Effect of Surface Active Organics. *J. Phys. Chem. A* **2005**, *109*, 10004–10012.
- (7) Cosman, L. M.; Knopf, D. A.; Bertram, A. K.  $\text{N}_2\text{O}_5$  Reactive Uptake on Aqueous Sulfuric Acid Solutions Coated with Branched and Straight-Chain Insoluble Organic Surfactants. *J. Phys. Chem. A* **2008**, *112*, 2386–2396.
- (8) Duffey, K. C.; Shih, O.; Wong, N. L.; Drisdell, W. S.; Saykally, R. J.; Cohen, R. C. Evaporation Kinetics of Aqueous Acetic Acid Droplets: Effects of Soluble Organic Aerosol Components on the Mechanism of Water Evaporation. *Phys. Chem. Chem. Phys.* **2013**, *15*, 11634–11639.
- (9) Park, S.-C.; Burden, D. K.; Nathanson, G. M. Surfactant Control of Gas Transport and Reactions at the Surface of Sulfuric Acid. *Acc. Chem. Res.* **2009**, *42*, 379–387.

- (10) Winter, B.; Weber, R.; Schmidt, P. M.; Hertel, I. V.; Faubel, M.; Vrbka, L.; Jungwirth, P. Molecular Structure of Surface-Active Salt Solutions: Photoelectron Spectroscopy and Molecular Dynamics Simulations of Aqueous Tetrabutylammonium Iodide. *J. Phys. Chem. B* **2004**, *108*, 14558–14564.
- (11) Brastad, S. M.; Albert, D. R.; Huang, M.; Nathanson, G. M. Collisions of DCI with a Solution Covered with Hydrophobic and Hydrophilic Ions: Tetrahexylammonium Bromide in Glycerol. *J. Phys. Chem. A* **2009**, *113*, 7422–7430.
- (12) Wang, C.-Y.; Morgner, H. Surface Structure of Cationic Surfactant Solutions Investigated by Angular Resolved X-Ray Photoelectron Spectroscopy with Calibrated Transmission Function. *Surf. Interface Anal.* **2011**, *43*, 784–790.
- (13) Kikkawa, N.; Ishiyama, T.; Morita, A. Molecular Dynamics Study of Phase Transfer Catalyst for Ion Transfer Through Water-Chloroform Interface. *Chem. Phys. Lett.* **2012**, *534*, 19–22.
- (14) Benjamin, I. Recombination, Dissociation, and Transport of Ion Pairs across the Liquid/Liquid Interface. Implications for Phase Transfer Catalysis. *J. Phys. Chem. B* **2013**, *117*, 4325–4331.
- (15) Ghosal, S.; Hemminger, J. C.; Bluhm, H.; Mun, B. S.; Hebenstreit, E. L. D.; Ketteler, G.; Olgetree, D. F.; Requejo, F. G.; Salmeron, M. Electron Spectroscopy of Aqueous Solution Interfaces Reveals Surface Enhancement of Halides. *Science* **2005**, *307*, 563–566.
- (16) Petersen, P. B.; Saykally, R. J. On the Nature of Ions at the Liquid Water Surface. *Annu. Rev. Phys. Chem.* **2006**, *57*, 333–64.
- (17) Gopalakrishnan, S.; Liu, D. F.; Allen, H. C.; Kuo, M.; Shultz, M. J. Vibrational Spectroscopic Studies of Aqueous Interfaces: Salts, Acids, Bases, and Nanodrops. *Chem. Rev.* **2006**, *106*, 1155–1175.
- (18) Jungwirth, P.; Tobias, D. J. Specific Ion Effects at the Air/Water Interface. *Chem. Rev.* **2006**, *106*, 1259–1281.
- (19) Andersson, G.; Krebs, T.; Morgner, H. Angle Resolved Ion Scattering Spectroscopy Reveals the Local Topography Around Atoms in a Liquid Surface. *Phys. Chem. Chem. Phys.* **2005**, *7*, 2948–2954.
- (20) Hu, J. H.; Shi, Q.; Davidovits, P.; Worsnop, D. R.; Zahniser, M. S.; Kolb, C. E. Reactive Uptake of  $\text{Cl}_2(\text{g})$  and  $\text{Br}_2(\text{g})$  by Aqueous Surfaces as a Function of  $\text{Br}^-$  and  $\text{I}^-$  Ion Concentration: The Effect of Chemical Reaction at the Interface. *J. Phys. Chem.* **1995**, *99*, 8768–8776.
- (21) Thomas, J. L.; Jimenez-Aranda, A.; Finlayson-Pitts, B. J.; Dabdub, D. Gas-Phase Molecular Halogen Formation. *J. Phys. Chem. A* **2006**, *110*, 1859–1867.
- (22) Katrib, Y.; Deiber, G.; Schweitzer, F.; Mirabel, P.; George, C. Chemical Transformation of Bromine Chloride at the Air/Water Interface. *J. Aerosol Sci.* **2001**, *32*, 893–911.
- (23) Enami, S.; Vecitis, C. D.; Cheng, J.; Hoffmann, M. R.; Colussi, A. J. Electrospray Mass Spectrometric Detection of Products and Short-Lived Intermediates in Aqueous Aerosol Microdroplets Exposed to a Reactive Gas. *J. Phys. Chem. A* **2007**, *111*, 13032–13037.
- (24) Hunt, S. W.; Roeselová, M.; Wang, W.; Wingen, L. M.; Knipping, E. M.; Tobias, D. J.; Dabdub, D.; Finlayson-Pitts, B. J. Formation of Molecular Bromine from the Reaction of Ozone with Deliquesced NaBr Aerosol: Evidence for Interfacial Chemistry. *J. Phys. Chem. A* **2004**, *108*, 11559–72.
- (25) Margerum, D. W.; Gray, E. T.; Huffman, R. P. Chlorination and the Formation of N-Chloro Compounds in Water Treatment. In *Organometals and Organometalloids: Occurrence and Fate in the Environment*; Brinckman, F. E., Bellama, J. M., Eds.; American Chemical Society: Washington, DC, 1979; Vol. 82, pp 278–289.
- (26) Ershov, B. G.; Kelm, M.; Janata, E.; Gordeev, A. V.; Bohnert, E. Radiation-Chemical Effects in the Near-Field of a Final Disposal Site: Role of Bromine on the Radiolytic Processes in NaCl-Solutions. *Radiochim. Acta* **2002**, *90*, 617–622.
- (27) Dempsey, L. P.; Faust, J. A.; Nathanson, G. M. Near-Interfacial Halogen Atom Exchange in Collisions of  $\text{Cl}_2$  with 2.7 M NaBr-Glycerol. *J. Phys. Chem. B* **2012**, *116*, 12306–12318.
- (28) Seeley, J. V.; Morris, R. A.; Viggiano, A. A. Gas Phase Reactions of Hydrated Halides with Chlorine. *J. Phys. Chem.* **1996**, *100*, 15821–15826.
- (29) Huff, A. K.; Abbatt, J. P. D. Gas-Phase  $\text{Br}_2$  Production in Heterogeneous Reactions of  $\text{Cl}_2$ , HOCl, and BrCl with Halide-Ice Surfaces. *J. Phys. Chem. A* **2000**, *104*, 7284–7293.
- (30) Finlayson-Pitts, B. J. Tropospheric Chemistry of Sea Salt. *Chem. Rev.* **2003**, *103*, 4801–4822.
- (31) Rossi, M. J. Heterogeneous Reactions on Salts. *Chem. Rev.* **2003**, *103*, 4823–4882.
- (32) Foster, K. L.; Plastridge, R. A.; Bottenheim, J. W.; Shepson, P. B.; Finlayson-Pitts, B. J.; Spicer, C. W. The Role of  $\text{Br}_2$  and BrCl in Surface Ozone Destruction at Polar Sunrise. *Science* **2001**, *291*, 471–474.
- (33) Simpson, W. R.; von Glasow, R.; Riedel, K.; Anderson, P.; Ariya, P.; Bottenheim, J.; Burrows, J.; Carpenter, L. J.; Frieß, U.; Goodsite, M. E.; Heard, D.; Hutterli, M.; Jacobi, H.-W.; Kaleschke, L.; Neff, B.; Plane, J.; Platt, U.; Richter, A.; Roscoe, H.; Sander, R.; Shepson, P.; Sodeau, J.; Steffen, A.; Wagner, T.; Wolff, E. Halogens and Their Role in Polar Boundary-Layer Ozone Depletion. *Atmos. Chem. Phys.* **2007**, *7*, 4375–4418.
- (34) Cedzynska, K. Properties of Modified Electrolyte for Zinc-Bromine Cells. *Electrochim. Acta* **1995**, *40*, 971–976.
- (35) Miner, C. S. *Glycerol*; Reinhold Publishing Corporation: New York, 1953.
- (36) The  $\text{THA}^+$  surface excess of  $8 \times 10^{13} \text{ cm}^{-2}$  was calculated for an activity coefficient  $f_{\pm}$  of 1. If we assume that  $f_{\pm} = 0.7$ , then the surface excess rises slightly to  $\sim 9 \times 10^{13} \text{ cm}^{-2}$ . Our rough estimate of  $f_{\pm}$  comes from the activity of tetrabutylammonium iodide (TBAI) in water at 298 K: Marcus, Y. *J. Chem. Thermodyn.* **2008**, *40*, 1314–1317.
- (37) Morris, J. R.; Behr, P.; Antman, M. D.; Ringeisen, B. R.; Splan, J.; Nathanson, G. M. Molecular Beam Scattering from Supercooled Sulfuric Acid: Collisions of HCl, HBr, and  $\text{HNO}_3$  with 70 wt %  $\text{D}_2\text{SO}_4$ . *J. Phys. Chem. A* **2000**, *104*, 6738–6751.
- (38) The only study we could find that investigated reactions between  $\text{Cl}_2$  and protonated amines concerned primary alkylamines ( $\text{RNH}_3^+$ ), which were reported not to react with  $\text{Cl}_2$ . See ref 25.
- (39) As shown in ref 27,  $\text{Cl}_2$  resides in pure glycerol for microseconds or less without reacting before it desorbs into vacuum. The residence time of  $\text{Cl}_2$  in THABr-glycerol is not likely to be significantly altered by the hydrocarbon chains of  $\text{THA}^+$ . Equation 2 predicts that  $\tau$  is much smaller than 1 microsecond for  $\text{Cl}_2$  in heptane given an experimental solubility of  $\sim 1 \text{ M atm}^{-1}$  and assuming  $\beta \approx 1$  and  $D \approx 10^{-5} \text{ cm}^2 \text{ s}^{-1}$ . See: *Sulfur Dioxide, Chlorine, Fluorine and Chlorine Oxides; Solubility Data Series*; Young, C. L., Ed.; Pergamon: Oxford, **1983**, Vol. 12, pp 354–373.
- (40) Shi, Q.; Davidovits, P.; Jayne, J. T.; Worsnop, D. R.; Kolb, C. E. Uptake of Gas-Phase Ammonia. I. Uptake by Aqueous Surfaces as a Function of pH. *J. Phys. Chem. A* **1999**, *103*, 8812–8823.
- (41) The residence time analysis presented here applies only to absorption and desorption in the absence of reaction. The analysis can be extended to include the irreversible reaction  $\text{Cl}_2 + \text{Br}^- \rightarrow \text{Cl}_2\text{Br}^-$  with bulk-phase rate constant  $k$ , as described in the Appendices of refs 27 (p 12315) and 40 (p 8821). In the model case when the  $\text{Cl}_2$  pre- and postchopper spectra are identical and can be fit with  $\tau < 10^{-7} \text{ s}$  for  $k = 0$ , we find alternatively that  $k > 10^6 \text{ s}^{-1}$  for long  $\tau$ . The uptake of  $\text{Cl}_2$  with interfacial  $\text{Br}^-$  most likely combines a short residence time and fast reaction with  $\text{Br}^-$  in the interfacial region, as presented in the Discussion.
- (42) This 0.1 s characteristic residence time is likely to be a lower limit because it falls within the same time scale as the 0.12 s exposure time. As a result, some of the incident  $\text{Br}_2$  molecules will remain dissolved in solution as the postchopper spectrum is recorded, and the signal will be artificially lowered. The prechopper spectrum is not affected because the 80  $\mu\text{s}$  pulse width is much shorter than the exposure time. The residence time will therefore be even longer than 0.1 s when an increased postchopper/prechopper signal ratio is taken into account, but simulations indicate that such large ratios do not sensitively determine  $\tau$ , and we can only say that it exceeds 0.1 s.
- (43) Heyda, J.; Lund, M.; Ončák, M.; Slavíček, P.; Jungwirth, P. Reversal of Hofmeister Ordering for Pairing of  $\text{NH}_4^+$  vs Alkylated

Ammonium Cations with Halide Anions in Water. *J. Phys. Chem. B* **2010**, *114*, 10843–10852.

(44) Morgner, H.; Obergrodhage, J.; Richter, K.; Roth, K. The Solution of Tetrabutylammonium Iodide in Formamide: Investigation of the Surface by MIES. *J. Phys.: Condens. Matter* **1991**, *3*, 5639–5655.

(45) Liu, D.; Ma, G.; Levering, L. M.; Allen, H. C. Vibrational Spectroscopy of Aqueous Sodium Halide Solutions and Air-Liquid Interfaces: Observations of Increased Interfacial Depth. *J. Phys. Chem. B* **2004**, *108*, 2252–2260.

(46) Ghosal, S.; Brown, M. A.; Bluhm, H.; Krisch, M. J.; Salmeron, M.; Jungwirth, P.; Hemminger, J. C. Ion Partitioning at the Liquid/Vapor Interface of a Multicomponent Alkali Halide Solution: A Model for Aqueous Sea Salt Aerosols. *J. Phys. Chem. A* **2008**, *112*, 12378–12384.

(47) Liu, Q.; Margerum, D. W. Equilibrium and Kinetics of Bromine Chloride Hydrolysis. *Environ. Sci. Technol.* **2001**, *35*, 1127–1133.

(48) Bartlett, W. P.; Margerum, D. W. Temperature Dependencies of the Henry's Law Constant and the Aqueous Phase Dissociation Constant of Bromine Chloride. *Environ. Sci. Technol.* **1999**, *33*, 3410–3414.

(49) We imagine that  $\text{THA}^+\text{Br}_3^-$  first forms in the interfacial region from reaction between  $\text{Br}_2$  and  $\text{Br}^-$ , in analogy with  $\text{Cl}_2\text{Br}^-$  formation from  $\text{Cl}_2$  and  $\text{Br}^-$ , and then diffuses into solution as  $\text{THA}^+\text{Br}_3^-$ . The interfacial lifetime of this ion pair can be estimated from the time to jump one diameter from the subsurface to the surface, which is roughly given by  $l^2/D$ , where  $l \approx 10 \text{ \AA}$  is the length of the ion and  $D \approx 10^{-9} \text{ cm}^2 \text{ s}^{-1}$ . The time for desorption of  $\text{THA}^+\text{Br}_3^-$  from the surface into the subsurface is then  $\sim 10 \mu\text{s}$ . If  $\text{THA}^+$  segregates to the surface as a monolayer, the surface to subsurface concentration ratio is roughly 100:1 (ref 11). Accordingly, the reverse time for  $\text{THA}^+$  to move one diameter from the surface to the subsurface should be about 1 ms. This time is much shorter than the  $\text{Br}_3^-$  lifetime of 0.1 s, implying that its enhanced solubility is not a surface-specific phenomenon even though  $\text{Br}_3^-$  is likely to be created in the interfacial region.

(50) Collins, K. D. Ion Hydration: Implications for Cellular Function, Polyelectrolytes, and Protein Crystallization. *Biophys. Chem.* **2006**, *119*, 271–281.

(51) Lund, M.; Jagoda-Cwiklik, B.; Woodward, C. E.; Vácha, R.; Jungwirth, P. Dielectric Interpretation of Specificity of Ion Pairing in Water. *J. Phys. Chem. Lett.* **2010**, *1*, 300–303.

(52) Landrum, G. A.; Goldberg, N.; Hoffmann, R. Bonding in the Trihalides ( $\text{X}_3^-$ ), Mixed Trihalides ( $\text{X}_2\text{Y}^-$ ) and Hydrogen Bihalides ( $\text{X}_2\text{H}^-$ ). The Connection Between Hypervalent, Electron-Rich Three-Center, Donor-Acceptor and Strong Hydrogen Bonding. *J. Chem. Soc., Dalton Trans.* **1997**, 3605–3613.

(53) Coleman, A. W.; Means, C. M.; Bott, S. G.; Atwood, J. L. Air-Stable Liquid Clathrates. 1. Crystal Structure of  $[\text{NBu}_4][\text{Br}_3]$  and Reactivity of the  $[\text{NBu}_4][\text{Br}_3] \cdot \text{S C}_6\text{H}_6$  Liquid Clathrate. *J. Cryst. Spectrosc.* **1990**, *20*, 199–201.

(54) Winter, B.; Weber, R.; Hertel, I. V.; Faubel, M.; Vrbka, L.; Jungwirth, P. Effect of Bromide on the Interfacial Structure of Aqueous Tetrabutylammonium Iodide: Photoelectron Spectroscopy and Molecular Dynamics Simulations. *Chem. Phys. Lett.* **2005**, *410*, 222–227.

(55) Reeser, D. I.; Donaldson, D. J. Influence of Water Surface Properties on the Heterogeneous Reaction Between  $\text{O}_3(\text{g})$  and  $\text{I}^-(\text{aq})$ . *Atmos. Environ.* **2011**, *45*, 6116–6120.

(56) Mmereki, B. T.; Donaldson, D. J.; Gilman, J. B.; Eliason, T. L.; Vaida, V. Kinetics and Products of the Reaction of Gas-Phase Ozone with Anthracene Adsorbed at the Air-Aqueous Interface. *Atmos. Environ.* **2004**, *38*, 6091–6103.

(57) Faubel, M.; Schlemmer, S.; Toennies, J. P. A Molecular Beam Study of the Evaporation of Water from a Liquid Jet. *Z. Phys. D* **1988**, *10*, 269–277.

(58) Ringeisen, B. R.; Muenter, A. H.; Nathanson, G. M. Collisions of  $\text{HCl}$ ,  $\text{DCl}$ , and  $\text{HBr}$  with Liquid Glycerol: Gas Uptake,  $\text{D} \rightarrow \text{H}$  Exchange, and Solution Thermodynamics. *J. Phys. Chem. B* **2002**, *106*, 4988–4998.